Characterization of RA839, a Noncovalent Small Molecule Binder to Keap1 and Selective Activator of Nrf2 Signaling*⒮

Angelika F. Winkel[‡], Christian K. Engel[‡], Daniel Margerie[‡], Aimo Kannt[‡§], Hauke Szillat[‡], Heiner Glombik[‡], Christopher Kallus[‡], Sven Ruf[‡], Stefan Güssregen[‡], Jens Riedel[‡], Andreas W. Herling[‡], Andreas von Knethen[¶], Andreas Weigert[¶], Bernhard Brüne[¶], and Dieter Schmoll[‡1]

From the ‡R&D, Sanofi, 65926 Frankfurt, Germany, the §Medical Faculty Mannheim, Heidelberg University, 69120 Mannheim, Germany, the ¶Faculty of Medicine, Biochemistry I, Goethe-University Frankfurt, 60590 Frankfurt, Germany

The activation of the transcription factor NF-E2-related factor 2 (Nrf2) maintains cellular homeostasis in response to oxidative stress by the regulation of multiple cytoprotective genes. Without stressors, the activity of Nrf2 is inhibited by its interaction with the Keap1 (kelch-like ECH-associated protein 1). Here, we describe (3S)-1-[4-[(2,3,5,6-tetramethylphenyl) sulfonylamino]-1-naphthyl]pyrrolidine-3-carboxylic acid (RA839), a small molecule that binds noncovalently to the Nrf2-interacting kelch domain of Keap1 with a K_d of ~6 μM, as demonstrated by x-ray co-crystallization and isothermal titration calorimetry. Whole genome DNA arrays showed that at 10 μM RA839 significantly regulated 105 probe sets in bone marrow-derived macrophages. Canonical pathway mapping of these probe sets revealed an activation of pathways linked with Nrf2 signaling. These pathways were also activated after the activation of Nrf2 by the silencing of Keap1 expression. RA839 regulated only two genes in Nrf2 knock-out macrophages. Similar to the activation of Nrf2 by either silencing of Keap1 expression or by the reactive compound 2-cyano-3,12-dioxooleana-1,9-dien-28-oic acid methyl ester (CDDO-Me), RA839 prevented the induction of both inducible nitric-oxide synthase expression and nitric oxide release in response to lipopolysaccharides in macrophages. In mice, RA839 acutely induced Nrf2 target gene expression in liver. RA839 is a selective inhibitor of the Keap1/Nrf2 interaction and a useful tool compound to study the biology of Nrf2.

The transcription factor NF-E2-related factor 2 (Nrf2)[2] is a promising target for the treatment of oxidative and inflammatory stress-related disorders, such as neurodegenerative and microvascular diseases (1–5). Nrf2 regulates the expression of several cytoprotective anti-oxidative and anti-inflammatory proteins by binding to the *cis*-acting antioxidant response element (ARE) within gene promoters. Nrf2 itself is regulated by the kelch-like ECH-associated protein 1 (Keap1), which is a substrate recognition subunit for a cullin3-based ubiquitin E3 ligase and functions as a sensor for oxidative and electrophilic stress. Structural elements of the Keap1 protein include the C-terminal Nrf2-binding kelch domain, the intervening region, and the broad complex-Tramtrack-Bric-a-Brac domain. Keap1 binds as a dimer via its two Kelch domains to one molecule of Nrf2, specifically to the high affinity ETGE and the low affinity DLG motives at the N terminus of Nrf2. Without stressors, this leads to the ubiquitinylation and subsequent proteolytic degradation of the transcription factor. In the presence of oxidative or electrophilic stress, cysteine residues within the intervening region and broad complex-Tramtrack-Bric-a-Brac domain of Keap1 become modified. According to the hinge and latch model, this weakens the interaction between Keap1 and the DLG motif of Nrf2 but does not lead to a release of Nrf2 (6, 7). The conformation cycling model postulates a stabilization of the Keap1/Nrf2 interaction by the Keap1 modification, which prevents the release of Nrf2 (8). With that, both models propose that newly synthesized Nrf2 is not degraded but translocates to the nucleus. Pharmacological Nrf2 activators, such as dimethyl fumarate, oltipraz, 2-cyano-3,12-dioxooleana-1,9-dien-28-oic acid methyl ester (CDDO-Me, Bardoxolone-Me), and sulforaphane also covalently modify the reactive cysteine residues of Keap1 (9–14). Clinical trials indicate beneficial efficacy of some of these covalent Nrf2 activators (15, 16). However, either serious safety issues were observed (17) or the contribution of Nrf2 activation to the clinical effect was unclear because of an unselective activity (18). Noncovalent inhibitors of Keap1 could be superior to covalent Keap1 binders with respect to toxicity because of their reversible and potentially more selective mode of action (19). Recently, small molecule binders to the Kelch domain of Keap1 were described that prevent the interaction between Keap1 and Nrf2 in binding assays (20–22). These molecules also possess cellular activity measured by either reporter gene induction or the activation of selected stress response genes that are, however, also regulated by mechanisms in addition to Nrf2. Despite these achievements, it is unknown whether direct inhibition of the Keap1/Nrf2 interaction is indeed able to stimulate Nrf2-dependent gene expression with high selectivity, as well as to exhibit cellular effects similar to those that have been attributed to the covalent Keap1 inhibitors. We therefore set out to search for a small molecule noncovalent binder to the Keap1 kelch domain with Nrf2-depen-

---

dent biological activity. We identified compound RA839, the characterization of which is described in the present study.

Experimental Procedures

Animal Study—The study was performed under the terms of the German Animal Protection Law, as well as according to international animal welfare legislation and rules and in accordance with the Sanofi Company Charter on the Humane Care and Use of Laboratory Animals.

Male mice (C57/Bl 6) with a body weight of about 22 g were housed in standard Makrolon cages type III at 22 ± 2 °C and 45–65% humidity under a normal light-dark cycle (light off 1800–0600) for at least 7 days on standard chow (Ssniff R/M) for acclimatization prior to the experiment. Three groups ($n = 8$) of mice were used for the study. On the study day, the mice were starved for 3 h prior to the start of treatment. As the test compound was metabolically labile, it was tested in the presence of 1-aminobenzotriazole (ABT), a nonspecific total inhibitor of cytochrome P450 enzymes. ABT was dissolved in saline and administered at 50 mg/kg per gavage 1 h prior to the administration of RA839. The compound was dissolved in 95% (v/v) hydroxyethyl cellulose (0.5% (w/v))/5% (v/v) solutol and administered intraperitoneally at the dose of 30 mg/kg. Three hours later, the animals were euthanized in deep isoflurane anesthesia by terminal blood collection. Hepatic tissue samples were collected after laparotomy for subsequent RNA isolation.

Fluorescence Polarization (FP) Assay—An FP assay was used to measure binding of the human Keap1 kelch domain (amino acids Ala[321]–Thr[609]) to a fluorescently labeled peptide containing the Keap1 ETGE binding site of human Nrf2 (Alexa633-AFFAQLQLDEETGEFL; JPT Technologies). 2 μl of test compound in reaction buffer (PBS, 2 mM DL-DTT, 0.015% (v/v) Brij-35) containing 6% (v/v) DMSO were mixed with 2 μl of the Keap1 kelch domain in reaction buffer without DMSO in a black 384-well microtiter plate and incubated at ambient temperature for 15 min. Thereafter, 2 μl of the fluorescently labeled Nrf2 peptide in reaction buffer without DMSO were added, and the mixture was incubated for a further 30 min at ambient temperature. The final concentrations of the Keap1 kelch domain and the fluorescently labeled Nrf2 peptide were 20 and 50 nM, respectively. FP was measured at excitation and emission wavelengths of 635 and 660 nm, respectively. The sequence of the DLG peptide used for competition was ILWRQDIDLGVSREV.

Reporter Gene Assay and Nrf2 Translocation Assay—The ARE-luciferase reporter gene assay was carried out as described recently (23). Nuclear translocation of Nrf2 after an incubation time of 6 h was determined using the PathHunter U2OS Keap1-NRF2 nuclear translocation cell line (DiscoverX) following the manufacturer's instructions. Nrf2-ARE binding activity was determined in nuclear extracts of HepG2 cells using the TransAM Nrf2 kit (Actif Motif) as described (23). The specificity of binding was determined by competition with oligonucleotides that had the sequence of either the wild-type or the mutated ARE motif according to the manufacturer's instructions. The data are presented as the difference in the extinction measured in the presence of the noncompeting oligonucleotide

and the extinction that was determined in the presence of the competing oligonucleotide.

Incubations of Bone Marrow-derived Murine Macrophages (BMDM) and Cytotoxicity Assay—BMDM were generated from total bone marrow of 12-week-old $Nrf2^{+/+}$ and $Nrf2^{-/-}$ mice in the C57BL/6J background as described previously (24). Compounds were prepared as DMSO stock solutions and further diluted in growth medium (RPMI medium (Gibco) containing 10% heat-inactivated FBS (PAA Laboratories)). BMDM were incubated with the indicated concentrations of the compounds at a fixed DMSO concentration of 0.2% (v/v). For the gene array studies, the incubation time was 4 h, before RNA was isolated. In the case of the NO release assay, BMDM were preincubated for 1 h in the presence of the compounds before LPS from *Escherichia coli* (055:B5, Sigma) were added to a final concentration of 1 μg/ml. After 48 h, NO release was measured, and RNA was isolated for gene expression studies. Cell viability was determined by the determination of lactate dehydrogenase release using the Cytotox-ONE assay (Promega).

Transfection of BMDM with siRNAs—The transfection was performed in growth medium using GeneMute for primary macrophages (SignaGen) according to the manufacturer's instructions. One day post-transfection, the medium was exchanged for fresh medium with or without LPS, and cells were incubated for 48 h before either NO release was determined or RNA was isolated for gene expression studies. The following siRNAs were used: siKeap1-1 (Dharmacon, J-041104-09, target sequence GCGCCAAUGUUGACACGGA), siKeap1-2 (Qiagen, Mm_Keap1_7, target sequence TTCCTGCAACTCGGTGAT-CAA), and as a control the nonsilencing siControl (sequence UUUCGCGUAUACGCGAAACdTdT).

NO Release Assay—For the detection of NO release, cell supernatants were added to an equal volume of Griess reagent (Sigma). After an incubation of 15 min, the absorbance at 540 nm was determined.

Protein Production, Crystallization, and Structure Determination—The murine Keap1 Kelch-DC (309–624), which has 100% sequence identity within the Keap1 kelch binding site with the human protein, was expressed in *E. coli* BL21 and purified by nickel affinity chromatography and size exclusion chromatography in a final buffer of 20 mM Tris-HCl, pH 8.5, 20 mM DTT. The protein was concentrated to 5.5 mg/ml. Crystallization experiments were performed by using the hanging drop vapor diffusion method at 4 °C by mixing 1 μl of protein solution with 1 μl of reservoir solution containing 0.1 M sodium citrate, pH 5.5, 0.9 M lithium sulfate, and 0.5 M ammonium sulfate. For soaking experiments single crystals were transferred into a soaking solution containing 0.1 M sodium citrate, pH 5.5, 0.9 M lithium sulfate, 1.5 M ammonium sulfate, 25% (v/v) ethylene glycol, 10% (v/v) DMSO, and 10 mM RA839. After 4 days, crystals were harvested directly from the soaking solution and flash-frozen in liquid nitrogen. Data collection was performed at the Swiss Light Source. Data processing and structure refinement was performed as described (25). The coordinates and structures factors of the crystal structure were submitted to the Protein Data Bank (code 5CGJ).

In Vitro Binding Assay—The N-terminal domain of Nrf2 (1–96) was cloned in pET15, expressed in *E. coli* BL21 and purified via an N-terminal His tag (7). 10 μg of the protein were bound to 200 μl of HIS-select HF nickel affinity gel (Sigma) equilibrated in binding buffer (50 mM sodium phosphate buffer, pH 8.0, 150 mM NaCl) overnight at 4 °C followed by washing twice with binding buffer. The gel was resuspended in 250 μl of binding buffer. 50-μl aliquots of the gel were incubated with 1 μg of recombinant Flag-tagged Keap1 (OriGene) in the presence of 1% DMSO either without RA839 or in the presence of 1, 10, or 100 μM RA839 in a final volume of 70 μl for 5 h at room temperature. As a control, the Nrf2-loaded gel was incubated in the absence of Keap1. In addition, Keap1 was incubated with unloaded affinity gel. The reactions were washed three times with binding buffer, resuspended in SDS sample buffer (Invitrogen), and loaded on 16% Tris-glycine SDS gels (Invitrogen). SDS-PAGE and Western blotting were performed as described. The blots were incubated with anti-FLAG antibodies (Sigma) overnight at 4 °C. After washing they were incubated with peroxidase-conjugated anti-rabbit Ig for 1 h. Detection was performed by Lumi-Light Western blotting substrate (Sigma). Subsequently, the blots were stripped and reprobed with an antibody specific for His tag (Cell Signaling Technology). The molecular weights of samples were estimated using the Spectra multicolor marker (Sigma).

Selectivity Panels—The interactions of 10 μM RA839 with a panel of 93 receptors, ion channels, enzymes, and protein kinases (supplemental Table S1) were tested by Eurofins Cerep (France).

Isothermal Titration Calorimetry (ITC)—ITC measurements were carried out on a VP-ITC ultrasensitive titration calorimeter (MicroCal Inc., Northampton, MA) as described (26). The measuring cell contained 40 μM Keap1 kelch domain protein, and the syringe contained 400 μM ligand in binding buffer (60 mM sodium phosphate, 1 mM TCEP, pH 8.1). The titrant was either RA839 or the ETGE peptide with the sequence AFFA-QLQLDEETGEFL. Blank titrations of ligands into buffer were also performed to correct for heats generated by dilution and mixing. The heat evolved after each injection was obtained from the time integral of the calorimetric signal, and data were fit to a binding model using Origin version 7.0 (OriginLab Corp., Northampton, MA).

Reverse Transcription and Real Time PCR—Reverse transcription and real time PCR were performed as described previously (23) with the following primer sets: Mm00500821-m1 (NAD(P)H dehydrogenase, quinone 1 (*Nqo1*)), Mm00802655-m1 (glutamate-cysteine ligase, catalytic subunit (*Gclc*)), Mm00497269-m1(Keap1), Mm00440502-m1 (inducible nitric-oxide synthase (*Nos2*)) Mm00497268_m1 (*Keap1*), Mm00477784_m1 (*Nrf2*), and Mm01546394-s1 (*Rpl37a*). Quantification was performed using the δδCt method with RPL37a as internal standard.

Microarray Transcript Analysis—Comparative microarray analysis was performed using Mouse Genome 430 2.0 GeneChips (Affymetrix). Four replicates originating from four different mice were carried out, resulting in four independent microarrays for each individual treatment and control group. Total RNA from mouse macrophages was isolated, and the integrity of RNA samples was controlled by RNA nano assay (Agilent 2100 BioAnalyzer). First and second strand cDNA

syntheses were performed using SuperScript SSII RT polymerase system (Invitrogen). Biotin-UPT- and -CTP-labeled cRNA was transcribed *in vitro* using Enzo BioArray high yield RNA transcript labeling kit (Enzo Diagnostics). 15 μg of cRNA samples were fragmented, added to hybridization buffer, and hybridized to Affymetrix GeneChip. Microarrays were washed and double-stained with streptavidin-phycoerythrin conjugate (Molecular Probes), anti-streptavidin antibody, and again streptavidin-phycoerythrin conjugate and then scanned. Quality control of each chip was performed according the Affymetrix quality criteria, including mean average difference, raw intensity, and 3′/5′ ratio of housekeeping genes *β-actin* and *Gapdh*. Expression data were submitted to the NCBI GEO database (accession number GSE71695).

Bioinformatics Analysis and Ingenuity Pathway Analysis (IPA)—Bioinformatics analysis of the Affymetrix raw data were performed with the Array Studio software package (OmicSoft). For this, Affymetrix cel files were first processed with robust multiarray average as a normalization method, and the data were then log2 transformed. For detection of expressed genes all Affymetrix probe sets with intensity signals of <6 in at least 25% of the samples were filtered out. Principal component analysis was applied to all samples as a quality control measure. To detect differentially expressed genes, a pairwise ANOVA statistical test was applied between the treated and control groups. Criteria for determining differentially expressed genes with statistical significance were changes in expression levels higher than 2-fold and a p value <0.01. Pathway and global functional analyses of differentially expressed genes were performed using the IPA software (Qiagen). Data sets containing Affymetrix probe sets and corresponding expression values were uploaded into the application, and each gene identifier was mapped using the IPA library. Canonical pathway analysis identified the canonical pathways from the IPA library that were most significant to the data set. The significance of the association between the data set and the canonical pathway was measured in two ways: 1) a ratio of the number of molecules from the data set that map to the pathway divided by the total number of molecules that map to the canonical pathway and 2) Fisher's exact test to calculate a p value determining the probability that the association between the genes in the data set and the canonical pathway is explained by chance alone. The IPA downstream effects analysis was used to identify the biological functions that were most significant to the data set. Right-tailed Fisher's exact test was used to calculate a p value determining the probability that each biological function assigned to these data sets are due to chance alone. Furthermore, IPA downstream effects analysis was used to predict increases or decreases of these biological functions occurring in macrophages after treatment by integrating the direction change of the differentially expresses genes into a z score algorithm calculation.

Testing of Metabolic Stability—RA839 (5 μM) was incubated in duplicates for 20 min at 37 °C in liver microsomal fraction (1 mg/ml protein) of human, rat, and mouse in the presence or absence of NADPH co-factor (1 mM). The reaction was stopped by addition of five volumes of precooled acetonitrile. The concentration of RA839 was determined by LC-MS.
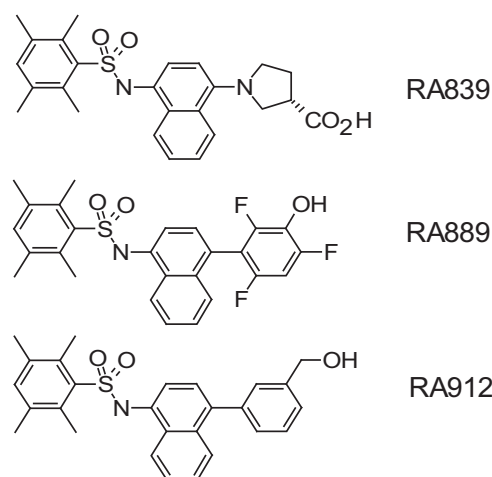
FIGURE 1. **Molecular structures of RA839, RA889, and RA912.**

FIGURE 2. *A–D*, characterization of molecules in a binding assay and cellular assays for Nrf2 activation. *A*, FP assay for binding of small molecules to the Keap1 kelch-domain. *B*, expression of a luciferase reporter gene driven by a promoter under control of ARE in HepG2 cells. *C*, Nrf2 translocation assay in U2OS cells. *Closed circles*, RA839; *asterisks*, RA889; *open circles*, RA912; *triangles*, CDDO-Me. The data are means + S.E. ($n = 6$). *D*, ARE binding activity in nuclear extracts of HepG2 cells; data are expressed as the difference in the absorption at 405 nm obtained in the presence of the noncompeting (*non-cp*) and the ARE sequence-competing oligonucleotide (*cp*) and are means of two independent experiments. *Closed circles*, RA839; *triangles*, CDDO-Me.

Results

Keap1 Kelch Domain Binding Characteristics of RA839— RA839 (Fig. 1 and supplemental text) was obtained by a screening effort followed by a medicinal chemistry program ((3S)-1-[4-[(2,3,5,6-tetramethylphenyl) sulfonylamino]-1-naphthyl] pyrrolidine-3-carboxylic acid) that will be described elsewhere. RA839 prevented the interaction of an Nrf2-derived peptide that included the sequence of Keap1 binding ETGE motif with the Keap1 kelch domain as determined by an FP assay with an IC$_{50}$ of 0.14 + 0.04 μM (mean ± S.D. $n = 6$) (Fig. 2*A*). Peptides with the sequences of the ETGE and the DLG motives had IC$_{50}$ values in this assay of 0.22 and >40 μM, respectively. Co-crystallization of RA839 with the Keap kelch domain revealed its binding mode (Fig. 3 and Table 1). The naphthalene ring system inserted deep into the central solvent channel of the kelch domain and the electron-rich ring formed stacking interactions with the Arg[415] side chain. The sulfonamide moiety formed a polar contact to Ser[602], placing the tetramethylphenyl-substituent into a hydrophobic and aromatic pocket of the Keap kelch binding site formed by Tyr[334], Phe[577], and Tyr[572]. The carboxylic group interacted directly with Arg[483]. The K_d of the interaction between the Keap kelch domain and RA839 amounted to 6 μM as determined by ITC, with a 1:1 stoichiometry of protein and ligand (Fig. 4 and Table 2). This is ~100-fold weaker than the binding of a 16-mer peptide with the ETGE sequence to the Kelch domain (Table 2). The thermodynamic profile showed that binding of RA839 to the kelch domain was driven by exothermic processes. This indicates a substantial contribution of ionic interaction to the overall binding, which is in line with the x-ray structure that demonstrated the interaction of RA839 with Arg[415] and Arg[483]. The significance of the interaction with Arg[483] is demonstrated by comparison with compounds RA889 and RA912 (Fig. 1) that were inactive in the FP assay (IC$_{50}$ > 10 μM) (Fig. 2*A*). These compounds are structurally related to RA839 but lack the carboxyl group that interacts with Arg[483]. The reactive Keap1 inhibitor CDDO-Me does not interact with the Keap1 kelch domain (11) and was, as expected, inactive in the binding assay (data not shown).

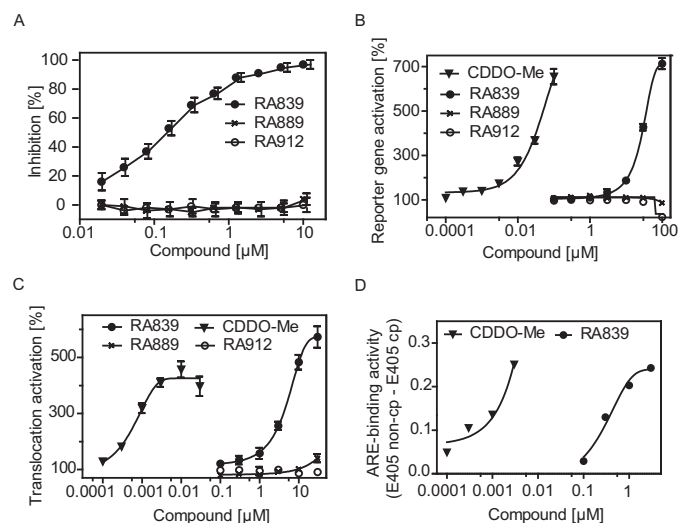Next we studied whether RA839 affects the interaction between full-length Keap1 and the N-terminal Nrf2 domain that comprises both Keap1 binding motifs (7), the ETGE and the DLG sequences. The N-terminal Nrf2 domain was immobilized to an affinity gel and incubated with recombinant Keap1. After washing of the gel and electrophoresis of the samples, binding of Keap1 to the immobilized Nrf2 domain could be detected, which was not affected by the presence of 10 μM of RA839 (Fig. 5). Even in the presence of 100 μM RA839 an interaction between Keap1 and the N-terminal domain of Nrf2 was detectable. Keap1 did not bind to the affinity gel in the absence of immobilized Nrf2 protein, and RA839 had no effect of the amount of Nrf2 immobilized to the gel.

Cellular Activity of RA839—RA839 induced both the luciferase expression driven by an ARE-containing promoter 5-fold at a concentration of 49 ± 8 μM (mean ± S.D., $n = 6$) (EC$_{500}$) in HepG2 cells and the nuclear localization of Nrf2 at a half-maximal concentration (EC$_{50}$) of 1.2 ± 0.3 μM (mean ± S.D., $n = 3$) in recombinant U2OS cells (Fig. 2, *B* and *C*). The covalent Keap1 inhibitor CDDO-Me was much more active than RA839, with an EC$_{500}$ of 0.07 ± 0.02 μM and an EC$_{50}$ of 3 ± 1 nM. RA889 and RA912 were inactive in the cellular assays with a cytotoxic effect of RA912 observed at 100 μM (Fig. 2, *B* and *C*). RA839 also increased the ARE binding activity in nuclear extracts of HepG2 cells, indicating nuclear accumulation of endogenous Nrf2 by RA839. Again, CDDO-Me was more potent than RA839 in the activation of Nrf2 (Fig. 2*D*). In the absence of an inductor, no specific nuclear ARE binding activity was detectable.

Selectivity of RA839—Next we tested whether the binding of RA839 to Keap1 and the subsequent translocation of the transcription factor Nrf2 regulates endogenous genes expression in primary BMDM. 10 μM RA839 significantly changed the expression of 105 probe sets in BMDM in relation to a vehicle control (Fig. 6 and supplemental Table S2). RA839 significantly
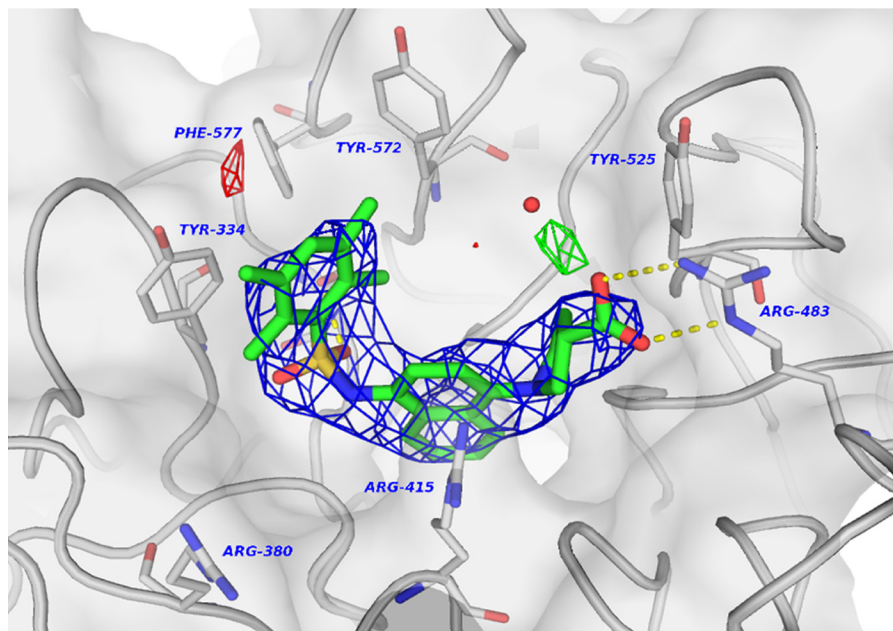
FIGURE 3. **Binding mode of RA839 (*green stick model*) in the Keap1 Kelch-DC.** Selected binding site residues are shown and labeled. The $2F_o - F_c$ electron density is drawn as a *blue mesh* around the ligand and contoured at 1σ. The $F_o - F_c$ electron density is shown as *green mesh* for positive difference density and *red mesh* for negative difference density, contoured at 3σ and -3σ, respectively. The figure was created by PyMOL.

TABLE 1
Data collection and refinement statistics
The values in parentheses correspond to the highest resolution shell.

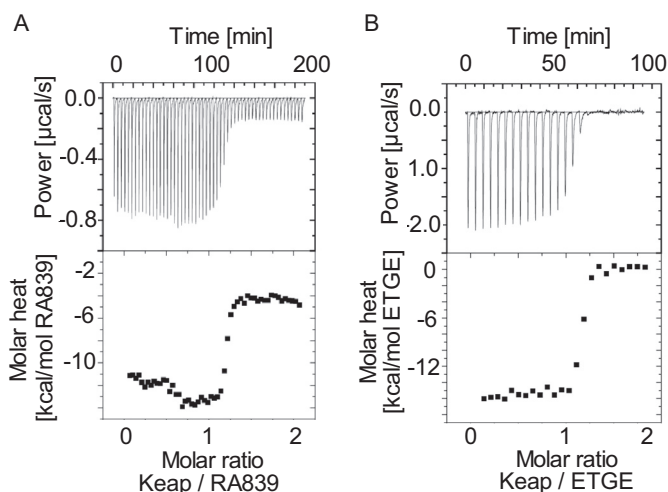|	RA839 complex
Data collection	
Space group	P61
a, b, c (Å)	103.131, 103.131, 56.141
α, β, γ (°)	90.00, 90.00, 120.00
Resolution (Å)	56.50–3.36 (3.37–3.36)
Unique reflections	5029 (39)
R_{merge} (%)	18.2 (53.8)
$I/\sigma(I)$	12.8 (4.2)
Completeness (%)	100 (100)
Redundancy	10.1 (9.6)
Temperature (K)	100
Refinement	
Resolution (Å)	51.71 − 3.36
No. reflections	5014
R_{work}/R_{free}	13.7/22.6
Protein	2226
Ligand	32
Solvent	13
Overall	49.5
Protein	49.0
Ligand	67.3
Solvent	16.2
Bonds (Å)	0.011
Angles (°)	1.27
Favoured (%)	91.0
Allowed (%)	6.2
Disallowed (%)	2.8

FIGURE 4. **Thermodynamics of the Keap1 kelch domain interactions with ligands.** Sample raw data for the titration of the kelch domain with either RA839 (*A*) or the ETGE peptide (*B*). *Top panels*, raw heating power data; *bottom panels*, data after peak integration, subtraction of blank titration data (not shown), and concentration normalization. Curve fit of the data to a single-site-binding model. 56 injections of 5 μl of RA839 and 23 injections of 10 μl of ETGE peptide were performed.

TABLE 2
Thermodynamic parameters of the Keap1 kelch domain interactions with RA839 and a peptide with the ETGE motif as ligands
The values are means ± S.E. ($n = 3$).

Ligand	K_d	ΔH	$T\Delta S$
	μM	kcal/mol	kcal/mol
RA839	6 ± 1.2	−28 ± 1.3	−22 ± 5
ETGE	0.038 ± 0.01	−15 ± 1.4	−5 ± 3

regulated only two genes, *Zfp192* and *Pank1*, in BMDM derived from *Nrf2* knock-out animals (supplemental Table S3). These genes were not regulated in wild-type macrophages. With that, RA839 regulates gene expression in a highly Nrf2-dependent manner in BMDM. The selectivity was further tested by mapping the regulated genes to canonical pathways. RA839 activated canonical Nrf2 signaling, as well as pathways of glutathione metabolism, which are well known to be regulated by Nrf2 (1), with the highest significance (Table 3). The mapping also indicated an activation of serine degradation, as well as eNOS

signaling by RA839. To further assess the selectivity of RA839 on gene expression, a genetic model for the activation of Nrf2 signaling was generated by silencing Keap1 expression using a siRNA approach. After the transient transfection of BMDM
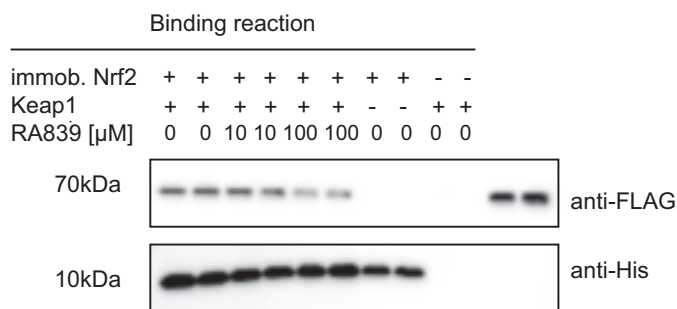
FIGURE 5. **Effect of RA839 on *in vitro* binding of Keap1 to the N-terminal domain of Nrf2.** Recombinant His-Nrf2 (1–98) was bound to an affinity gel and incubated in the presence or absence of recombinant Flag-Keap1 with or without RA839. After washing, samples were separated by SDS-PAGE. Immunoblots were stained for Flag-Keap1 and subsequently for His-Nrf2. As control, the interaction of Keap1 with the affinity gel in the absence of immobilized (*immob.*) His-Nrf2 domain was studied. For comparison, recombinant Flag-Keap1 was loaded. The experiment was repeated three times, and the results of two independent binding reactions are shown.
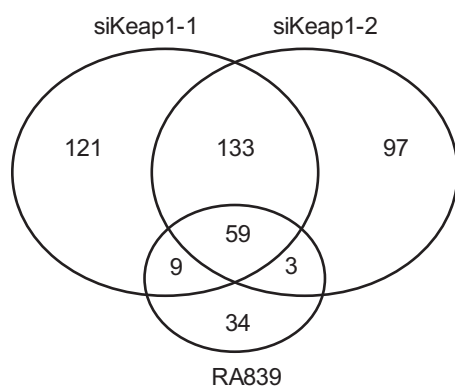

FIGURE 6. **Overlap of by siKeap1-1, siKeap1-2, and RA839 regulated probe sets (Venn diagram).** Those genes were analyzed that were regulated either by the transfection of BMDM with siKeap1-1 and siKeap1-2 in relation to nonsilencing siControl or by the incubation with 10 μM RA839 in relation to a vehicle control (fold-change >2, two-way ANOVA $p < 0.01$, $n = 4$).

with two different siRNAs against Keap1, siKeap1-1 and siKeap1-2, Keap1 expression was reduced by ~75 and 80%, respectively, *versus* a control siRNA. siKeap1-1 and siKeap1-2 regulated 292 probe sets and 322 probe sets, respectively, by more than 2-fold relative to siControl-transfected cells (Fig. 6). 192 probe sets were regulated by both *Keap1* siRNAs (supplemental Table S4). Pathway mapping of this set of overlapping genes (siKeap1 core) identified canonical Nrf2 signaling and glutathione metabolism as the most significantly regulated pathways, which were also regulated by RA839 (Table 3). In addition, the pathway analysis revealed the regulation of genes involved in the activation of white blood cells. These pathways were not significantly affected by RA839. Overall, 56% of the genes regulated by RA839 were also regulated by both siRNAs, and 68% of the genes were regulated by any of the siRNAs (Fig. 6). At a concentration of 10 μM, RA839 did not interact with a panel of 93 proteins that included unrelated enzymes, receptors, and channels (supplemental Table 1), further demonstrating selectivity of RA839 for Keap1 binding.

Anti-inflammatory Action of RA839—Reactive Nrf2-activating compounds such as CDDO-Me suppress the induction of NO production in macrophages (27). This assay was applied to assess the biological activity of RA839. The molecule reduced the LPS-induced NO release in BMDM in a concentration-dependent manner (Fig. 7*A*). CDDO-Me was active at a much lower concentration (Fig. 7*B*), which was expected from its higher potency in the cellular Nrf2 activation assays (Fig. 2, *A*–*D*). The treatment of macrophages with either RA839 or CDDO-Me did not affect cell viability, as measured by lactate dehydrogenase release into the supernatant (data not shown). The anti-inflammatory action of both RA839 and CDDO-Me coincided with their ability to inhibit the induction of *Nos2* expression by LPS in BMDM (Fig. 7*C*). Both RA839 and CDDO-Me stimulated the expression of the Nrf2 target gene *Nqo1* (Fig. 7*D*), indicating that LPS treatment had no general effect on the induction of Nrf2 target genes by the compounds. RA889 and RA912, which are structurally related to RA839 but did not activate Nrf2, affected neither the NO release nor the expression of *Nos2* and *Nqo1*, which suggests that the biological effect of RA839 is due to the activation of Nrf2. To assess the effect of genetic activation of Nrf2 on the inflammatory response of macrophages, Keap1 expression was silenced using two different siRNAs (Fig. 8*B*). Similar to the pharmacological activators of Nrf2, both siRNAs reduced NO release and NOS2 expression (Fig. 8, *A* and *C*). Both siRNAs increased the expression of the Nrf2 target gene *Nqo1* in the absence or presence of LPS (Fig. 8*D*), which demonstrates the activation of Nrf2 by the silencing of Keap1.

In Vitro Metabolism and in Vivo Activity of RA839—RA839 showed high rates of metabolic turnover of 99, 90, and 76% after 20-min incubation in liver microsomes from human, mouse, and rat, respectively, in the presence of co-factor NADPH. In the absence of NADPH, this value decreased to 51% in mouse microsomes, indicating a contribution of both oxidative and nonoxidative metabolism of RA839. To test the pharmacological *in vivo* activity of RA839 in mice, the compound was administered together with the cytochrome P450 inhibitor ABT, which reduces oxidative phase 1 metabolism. The hepatic mRNA levels of the prototypical Nrf2 target genes GCLC and NQO1 were significantly induced by RA839 3 h after the administration of RA839, whereas the expression of either Nrf2 or Keap1 did not change (Fig. 9). The addition of ABT had no effect by itself on the expression of these genes. This suggests that RA839 was able to regulate Nrf2 target genes *in vivo* after acute administration, if oxidative hepatic metabolism was reduced.

Discussion

We have demonstrated that it is possible to activate Nrf2 with high selectivity by a small molecule that binds noncovalently to the Keap1 kelch domain. A comparison of the x-ray co-crystal structure of the RA839-kelch domain complex with those reported for the kelch domain in complex with peptides possessing the sequence of either the ETGE and the DLG motifs of Nrf2 (7, 28) shows overlapping binding sites of the ligands. Our data indicate in particular a critical role of the ionic interaction of RA839 with Arg[483] of the Keap kelch domain, which is also addressed by the peptides. In our experiments, a short 16-mer peptide with the ETGTE sequence bound with high affinity to the Keap1 kelch domain ($K_d = 38$ nM). This is in agreement with data in the literature, in which K_d values of 5 nM and 1 μM, respectively, were reported (28) for the interaction of the ETGE and the DLG motifs of the Nrf2 N-terminal domain

TABLE 3
Canonical pathways regulated by RA839 and by both siKeap1-1 and siKeap1-2 (siKeap1 core)
Genes significantly regulated in BMDM by either 10 μM RA839 or silencing Keap1 expression by two different siRNAs were mapped by Ingenuity Pathway Analysis. The significance of the pathways is given as $-\log p$ value (Fisher's exact test).

| Canonical pathway	Statistical siginificance	Regulated genes
RA839		
Glutathione biosynthesis	7.7	*Gclc, Gclm, Gss*
γ-Glutamyl cycle	7.29	*Gclc, Ggt5, Gclm, Gss*
NRF2-mediated oxidative-stress response	5	*Gsta3, Gclc, Aox1, Gclm, Txnrd1, Mafg*
eNOS signaling	2.16	*Prkar2b, Prkaa2, Figf*
L-serine degradation	2.08E	*Srr*
siRNA core		
Nrf2-mediated oxidative stress response	6.6	*Gsta3, Gclc, Aox1, Gclm, Txnrd1, Mafg*
Glutathione biosynthesis	6.59	*Gclc, Gclm, Gss*
γ-Glutamyl cycle	5.81	*Gclc, Ggt5, Gclm, Gss*
Granulocyte adhesion and diapedesis	5.67	*Il36g, Cxcl1*
Agranulocyte adhesion and diapedesis	5.44	*Il36g, Cxcl1*
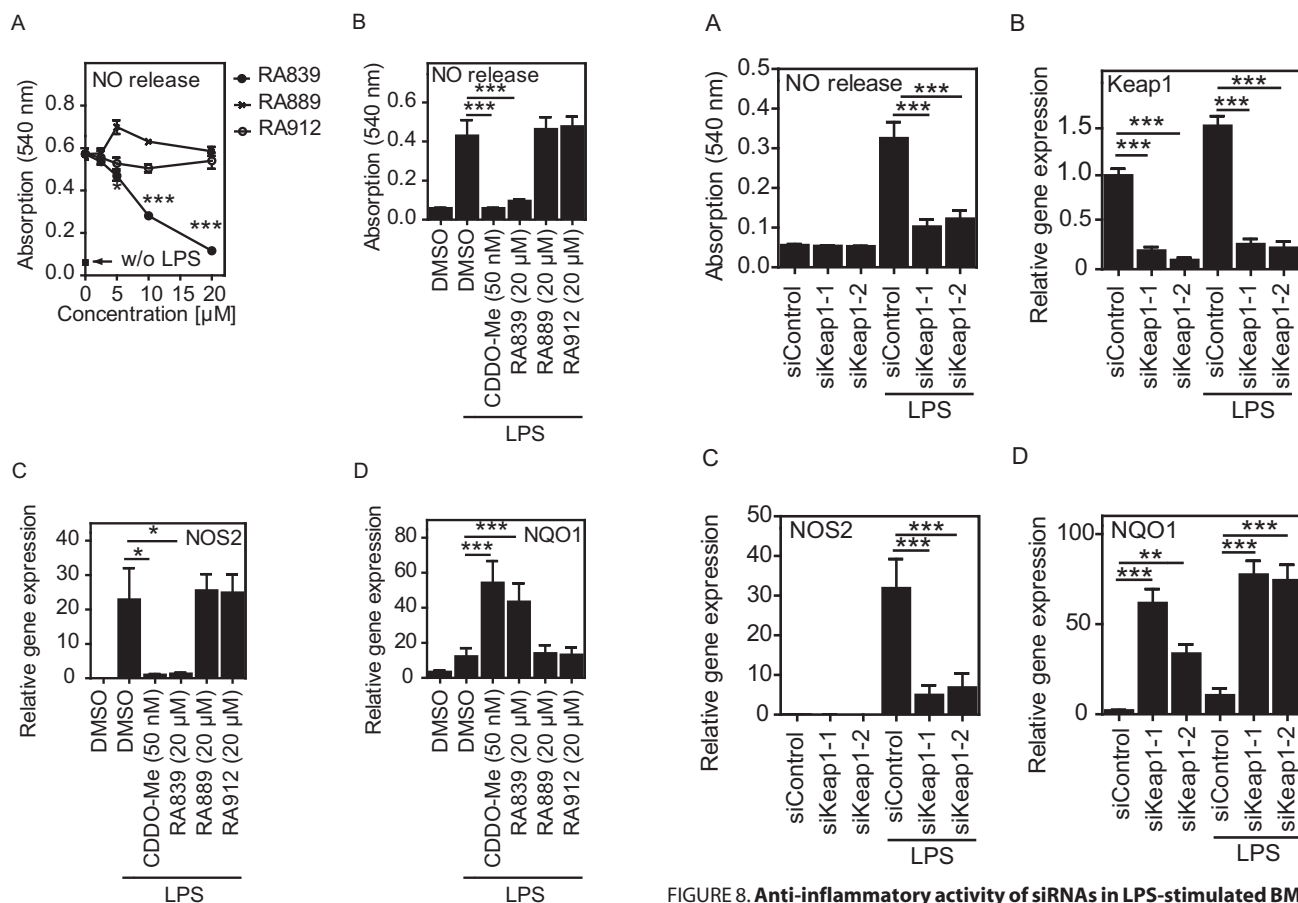
FIGURE 7. **Anti-inflammatory activity of small molecules in LPS-stimulated BMDM.** *A* and *B*, regulation of NO release determined by the absorption at 540 nm. *C* and *D*, regulation of *Nos2* (*C*) and *Nqo1* (*D*) expression as determined by quantitative RT-PCR in relation to the expression of *Rpl37a*. The data are means ± S.E. of three independent experiments carried out in duplicate, each with BMDM from two mice (one-way ANOVA). *, $p < 0.05$; ***, $p < 0.001$.

FIGURE 8. **Anti-inflammatory activity of siRNAs in LPS-stimulated BMDM.** *A*, suppression of LPS-induced NO release by siRNAs against *Keap1*. *B*, suppression of Keap1 expression by siRNAs against Keap1. *C*, suppression of *Nos2* expression in LPS-treated BMDM by siRNAs against *Keap1*. *D*, induction of *Nqo1* expression by siRNAs against *Keap1*. Gene expression was normalized by *Rpl37a* expression. The data are means ± S.E. of two independent experiments carried out in duplicates, each with BMDM from two mice (one-way ANOVA). **, $p < 0.01$; ***, $p < 0.001$.

with the Keap kelch domain. We determined a K_d value of 6 μM for the binding of RA839 using ITC. The IC$_{50}$ value of RA839 in the FP assay is very similar to that of a peptide with the ETGE motif, although the ITC data demonstrated an ~100-fold difference in the binding constants between RA839 and an ETGE peptide. Reasons for this could be a potential influence of the label in the FP assay or different binding conditions, *e.g.* the pH of the ITC binding buffer was significantly higher than the one used in the FP assay. *In vitro* even at a RA839 concentration of
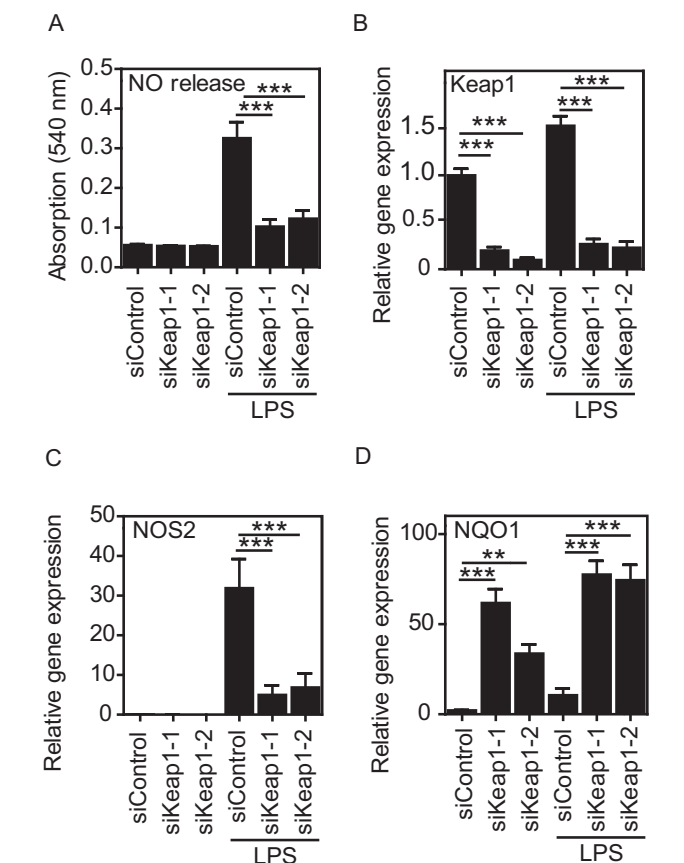
100 μM, an interaction between recombinant Keap1 and the N-terminal domain of Nrf2 was detectable. We speculate that at the concentrations used in the cell studies, RA839 affected mainly the weaker interaction between Keap1 and the DLG motif of Nrf2 and did not lead to a full dissociation. According to the hinge and latch model, as well as to the conformation cycling model, an interference of the interaction between Keap1 and the DLG motif of Nrf2 is already sufficient to prevent the degradation of Nrf2 (6, 8).
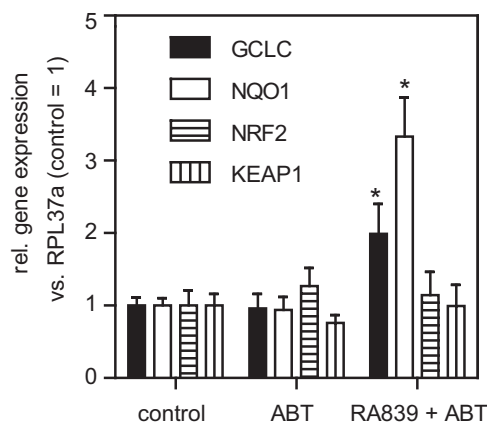
FIGURE 9. **Regulation of the Nrf2 target genes *Gclc* and *Nqo1* in mouse liver by RA839.** Mice were treated with or without RA839 and the pan-cytochrome P450 oxidase inhibitor ABT. After 3 h, the animals were killed, and RNA was isolated from liver. RNA levels of GCLC NQO1, Keap1, and Nrf2 in relation to RPL37a were determined by quantitative RT-PCR, controls were set as 1. The data are means $\pm$ S.E. ($n = 8$) (one-way ANOVA). *, $p < 0.05$ *versus* control.

The cellular activity of RA839 was determined in various assays and compared with that of CDDO-Me. The activity values for these compounds varied in the different assays because of different protocols and cannot be directly compared with each other. However, in all assays, RA839 was found to be $\sim 500-1000$-fold less potent than CDDO-Me. The selectivity of RA839 was demonstrated by binding studies using panels of unrelated proteins, as well as by gene expression studies with wild-type and Nrf2 knock-out BMDM. The only two genes (*Zfp192* and *Pank1*) that were regulated by RA839 in Nrf2 knock-out cells were not activated in wild-type BMDM. Further studies will have to elucidate how the regulation of these genes is affected by the genetic background. The mapping of the genes regulated by RA839 in wild-type BMDM demonstrated the activation of pathways directly linked to Nrf2 signaling, such as canonical Nrf2 signaling and glutathione metabolism (1) but also of eNOS signaling and serine degradation. Canonical serine degradation was mapped because of an up-regulation of a single gene, *Srr* (serine racemase). Further studies will have to show whether Nrf2 has a direct effect on *Srr* gene expression. The first evidence for this might come from the observation that serine racemase expression is regulated by oxidative stress (29). Although Nrf2 activation has not been directly associated with eNOS signaling, two genes (*Fifg* and *Prkaa2*) of this canonical pathway that were regulated by RA839 are regulated by Nrf2 and protect against oxidative stress, respectively (30–32). With that, their regulation most likely reflects a selective effect of the compound for the activation of Nrf2. The selectivity of RA839 was confirmed using a genetic model for Nrf2 activation. However, the absolute overlap of genes regulated by RA839 and by the siRNAs against *Keap1* was only moderate. Although we tried to minimize off-target effects of the respective siRNAs against *Keap1* by analyzing only those genes that were affected by both siRNAs, unselective effects of the siRNAs cannot be fully excluded. Evidence for this comes from the regulation of genes involved in macrophage activation by the siRNAs but not by RA839. In addition, the incubation time of BMDM

with the compound was only 4 h. Because of the methodology, gene expression was analyzed 48 h after transfection with the siRNAs, which might have led to secondary effects.

In our hands, three different approaches to activate Nrf2 via modulation of Keap1 activity suppressed the induction of *Nos2* expression by LPS in macrophages, *i.e.* blocking the Keap1 kelch domain by RA839, covalently modifying Keap1 by CDDO-Me and silencing *Keap1* expression by siRNAs. This strongly suggests that Nrf2 regulates *Nos2* expression in BMDM. In microglia cells, the activation of Nrf2 reduces *Nos2* expression by the recruitment of p300 co-activator (33). Further studies will have to show whether the same mechanism also functions in BMDM. Because of scarcity of sample material, we were not able to perform immunoblotting for *Nos2*. The observation that NO release was also suppressed by all three approaches strongly suggests that the change in *Nos2* gene expression has a functional role in BMDM.

The selectivity of RA839 makes it a useful tool compound for mechanistic studies and for defining both target-related and off-target effects of Nrf2-activating approaches. RA839 might also allow the identification of potentially different effects of covalent and noncovalent Keap1 inhibitors, *e.g.* RA839 could help to elucidate the biological role of the interaction between the Keap1 kelch domain and other proteins, such as p62 (34). Excessive oxidative stress and inflammation have been implicated in the progression of chronic diseases (4, 35, 36). The activation of Nrf2, which causes the stimulation of multiple endogenous anti-oxidative and anti-inflammatory pathways, could be a promising therapeutic approach (4). Existing pharmacological inhibitors of Keap1 such as CDDO-Me are reactive electrophilic molecules and have been shown to interact with other proteins in addition to Keap1 (37). Reactive molecules are prone to adverse off-target effects (19), and the reactive Nrf2 activators have shown adverse side effects in preclinical and clinical studies, respectively (36, 38–40). However, it is so far unknown whether these toxic effects are indeed caused by the unselective action of either the compounds or their metabolites or are elicited by chronic activation of Nrf2. RA839 is active *in vivo*, if oxidative metabolism is inhibited. Its metabolic instability prevented a chronic application. The present study demonstrates that it is possible to selectively activate Nrf2 by a noncovalent Keap1 binder. This may lay the basis for the identification of molecules with improved pharmacokinetics profile, which can be tested in models of chronic oxidative-stress related diseases. This will lead to a better understanding of the therapeutic potential of Nrf2 activation.

References

1. Hayes, J. D., and Dinkova-Kostova, A. T. (2014) The Nrf2 regulatory network provides an interface between redox and intermediary metabolism. *Trends Biochem. Sci.* **39,** 199–218

2. Suzuki, T., Motohashi, H., and Yamamoto, M. (2013) Toward clinical application of the Keap1-Nrf2 pathway. *Trends Pharmacol. Sci.* **34,** 340–346

3. Niture, S. K., Khatri, R., and Jaiswal, A. K. (2014) Regulation of Nrf2-an update. *Free Radic. Biol. Med.* **66,** 36–44

4. Gao, B., Doan, A., and Hybertson, B. M. (2014) The clinical potential of influencing Nrf2 signaling in degenerative and immunological disorders. *Clin. Pharmacol.* **6,** 19–34

5. Kwak, M. K., and Kensler, T. W. (2010) Targeting NRF2 signaling for cancer chemoprevention. *Toxicol. Appl. Pharmacol.* **244,** 66–76

6. Tong, K. I., Kobayashi, A., Katsuoka, F., and Yamamoto, M. (2006) Two-site substrate recognition model for the Keap1-Nrf2 system: a hinge and latch mechanism. *Biol. Chem.* **387,** 1311–1320

7. Tong, K. I., Padmanabhan, B., Kobayashi, A., Shang, C., Hirotsu, Y., Yokoyama, S., and Yamamoto, M. (2007) Different electrostatic potentials define ETGE and DLG motifs as hinge and latch in oxidative stress response. *Mol. Cell. Biol.* **27,** 7511–7521

8. Baird, L., Swift, S., Llères, D., and Dinkova-Kostova, A. T. (2014) Monitoring Keap1-Nrf2 interactions in single live cells. *Biotechnol. Adv.* **32,** 1133–1144

9. Liby, K. T., and Sporn, M. B. (2012) Synthetic oleanane triterpenoids: multifunctional drugs with a broad range of applications for prevention and treatment of chronic disease. *Pharmacol. Rev.* **64,** 972–1003

10. Scannevin, R. H., Chollate, S., Jung, M. Y., Shackett, M., Patel, H., Bista, P., Zeng, W., Ryan, S., Yamamoto, M., Lukashev, M., and Rhodes, K. J. (2012) Fumarates promote cytoprotection of central nervous system cells against oxidative stress via the nuclear factor (erythroid-derived 2)-like 2 pathway. *J. Pharmacol. Exp. Ther.* **341,** 274–284

11. Cleasby, A., Yon, J., Day, P. J., Richardson, C., Tickle, I. J., Williams, P. A., Callahan, J. F., Carr, R., Concha, N., Kerns, J. K., Qi, H., Sweitzer, T., Ward, P., and Davies, T. G. (2014) Structure of the BTB domain of Keap1 and its interaction with the triterpenoid antagonist CDDO. *PLoS One* **9,** e98896

12. Tran, Q. T., Xu, L., Phan, V., Goodwin, S. B., Rahman, M., Jin, V. X., Sutter, C. H., Roebuck, B. D., Kensler, T. W., George, E. O., and Sutter, T. R. (2009) Chemical genomics of cancer chemopreventive dithiolethiones. *Carcinogenesis* **30,** 480–486

13. Yates, M. S., and Kensler, T. W. (2007) Keap1 eye on the target: chemoprevention of liver cancer. *Acta Pharmacol. Sin.* **28,** 1331–1342

14. Takaya, K., Suzuki, T., Motohashi, H., Onodera, K., Satomi, S., Kensler, T. W., and Yamamoto, M. (2012) Validation of the multiple sensor mechanism of the Keap1-Nrf2 system. *Free Radic. Biol. Med.* **53,** 817–827

15. Pergola, P. E., Raskin, P., Toto, R. D., Meyer, C. J., Huff, J. W., Grossman, E. B., Krauth, M., Ruiz, S., Audhya, P., Christ-Schmidt, H., Wittes, J., Warnock, D. G., and BEAM Study Investigators (2011) Bardoxolone methyl and kidney function in CKD with type 2 diabetes. *N. Engl. J. Med.* **365,** 327–336

16. Gold, R., Kappos, L., Arnold, D. L., Bar-Or, A., Giovannoni, G., Selmaj, K., Tornatore, C., Sweetser, M. T., Yang, M., Sheikh, S. I., Dawson, K. T., and DEFINE Study Investigators (2012) Placebo-controlled phase 3 study of oral BG-12 for relapsing multiple sclerosis. *N. Engl. J. Med.* **367,** 1098–1107

17. de Zeeuw, D., Akizawa, T., Audhya, P., Bakris, G. L., Chin, M., Christ-Schmidt, H., Goldsberry, A., Houser, M., Krauth, M., Lambers Heerspink, H. J., McMurray, J. J., Meyer, C. J., Parving, H. H., Remuzzi, G., Toto, R. D., Vaziri, N. D., Wanner, C., Wittes, J., Wrolstad, D., Chertow, G. M., and BEACON Trial Investigators (2013) Bardoxolone methyl in type 2 diabetes and stage 4 chronic kidney disease. *N. Engl. J. Med.* **369,** 2492–2503

18. Chen, H., Assmann, J. C., Krenz, A., Rahman, M., Grimm, M., Karsten, C. M., Köhl, J., Offermanns, S., Wettschureck, N., and Schwaninger, M. (2014) Hydroxycarboxylic acid receptor 2 mediates dimethyl fumarate's protective effect in EAE. *J. Clin. Invest.* **124,** 2188–2192

19. Park, B. K., Boobis, A., Clarke, S., Goldring, C. E., Jones, D., Kenna, J. G., Lambert, C., Laverty, H. G., Naisbitt, D. J., Nelson, S., Nicoll-Griffith, D. A., Obach, R. S., Routledge, P., Smith, D. A., Tweedie, D. J., Vermeulen, N., Williams, D. P., Wilson, I. D., and Baillie, T. A. (2011) Managing the challenge of chemically reactive metabolites in drug development. *Nat. Rev. Drug Discov.* **10,** 292–306

20. Jiang, Z. Y., Lu, M. C., Xu, L. L., Yang, T. T., Xi, M. Y., Xu, X. L., Guo, X. K., Zhang, X. J., You, Q. D., and Sun, H. P. (2014) Discovery of potent Keap1-Nrf2 protein-protein interaction inhibitor based on molecular binding determinants analysis. *J. Med. Chem.* **57,** 2736–2745

21. Hu, L., Magesh, S., Chen, L., Wang, L., Lewis, T. A., Chen, Y., Khodier, C., Inoyama, D., Beamer, L. J., Emge, T. J., Shen, J., Kerrigan, J. E., Kong, A. N., Dandapani, S., Palmer, M., Schreiber, S. L., and Munoz, B. (2013) Discovery of a small-molecule inhibitor and cellular probe of Keap1-Nrf2 protein-protein interaction. *Bioorg. Med. Chem. Lett.* **23,** 3039–3043

22. Marcotte, D., Zeng, W., Hus, J. C., McKenzie, A., Hession, C., Jin, P., Bergeron, C., Lugovskoy, A., Enyedy, I., Cuervo, H., Wang, D., Atmanene, C., Roecklin, D., Vecchi, M., Vivat, V., Kraemer, J., Winkler, D., Hong, V., Chao, J., Lukashev, M., and Silvian, L. (2013) Small molecules inhibit the interaction of Nrf2 and the Keap1 Kelch domain through a non-covalent mechanism. *Bioorg. Med. Chem.* **21,** 4011–4019

23. Richter, M., Winkel, A. F., Schummer, D., Gerlitz, M., de Hoop, M., Brunner, B., Glien, M., and Schmoll, D. (2014) Pau d'arco activates Nrf2-dependent gene expression via the MEK/ERK-pathway. *J. Toxicol. Sci.* **39,** 353–361

24. Kuchler, L., Giegerich, A. K., Sha, L. K., Knape, T., Wong, M. S., Schröder, K., Brandes, R. P., Heide, H., Wittig, I., Brüne, B., and von Knethen, A. (2014) SYNCRIP-dependent Nox2 mRNA destabilization impairs ROS formation in M2-polarized macrophages. *Antioxid. Redox Signal.* **21,** 2483–2497

25. Halland, N., Brönstrup, M., Czech, J., Czechtizky, W., Evers, A., Follmann, M., Kohlmann, M., Schiell, M., Kurz, M., Schreuder, H. A., and Kallus, C. (2015) Novel small molecule inhibitors of activated thrombin activatable fibrinolysis inhibitor (TAFIa) from natural product anabaenopeptin. *J. Med. Chem.* **58,** 4839–4844

26. Anderka, O., Boyken, J., Aschenbach, U., Batzer, A., Boscheinen, O., and Schmoll, D. (2008) Biophysical characterization of the interaction between hepatic glucokinase and its regulatory protein: impact of physiological and pharmacological effectors. *J. Biol. Chem.* **283,** 31333–31340

27. Honda, T., Rounds, B. V., Bore, L., Finlay, H. J., Favaloro, F. G., Jr., Suh, N., Wang, Y., Sporn, M. B., and Gribble, G. W. (2000) Synthetic oleanane and ursane triterpenoids with modified rings A and C: a series of highly active inhibitors of nitric oxide production in mouse macrophages. *J. Med. Chem.* **43,** 4233–4246

28. Tong, K. I., Katoh, Y., Kusunoki, H., Itoh, K., Tanaka, T., and Yamamoto, M. (2006) Keap1 recruits Neh2 through binding to ETGE and DLG motifs: characterization of the two-site molecular recognition model. *Mol. Cell. Biol.* **26,** 2887–2900

29. Haxaire, C., Turpin, F. R., Potier, B., Kervern, M., Sinet, P. M., Barbanel, G., Mothet, J. P., Dutar, P., and Billard, J. M. (2012) Reversal of age-related oxidative stress prevents hippocampal synaptic plasticity deficits by protecting D-serine-dependent NMDA receptor activation. *Aging Cell* **11,** 336–344

30. Qiu, S. L., Xiao, Z. C., Piao, C. M., Xian, Y. L., Jia, L. X., Qi, Y. F., Han, J. H., Zhang, Y. Y., and Du, J. (2014) AMP-activated protein kinase α2 protects against liver injury from metastasized tumors via reduced glucose deprivation-induced oxidative stress. *J. Biol. Chem.* **289,** 9449–9459

31. Zong, J., Deng, W., Zhou, H., Bian, Z. Y., Dai, J., Yuan, Y., Zhang, J. Y., Zhang, R., Zhang, Y., Wu, Q. Q., Guo, H. P., Li, H. L., and Tang, Q. Z. (2013) 3,3′-Diindolylmethane protects against cardiac hypertrophy via 5′-adenosine monophosphate-activated protein kinase-alpha2. *PLoS One* **8,** e53427

32. Gjyshi, O., Bottero, V., Veettil, M. V., Dutta, S., Singh, V. V., Chikoti, L., and Chandran, B. (2014) Kaposi's sarcoma-associated herpesvirus induces Nrf2 during *de novo* infection of endothelial cells to create a microenvi-

ronment conducive to infection. *PLoS Pathog.* **10,** e1004460

33. Kim, S. W., Lee, H. K., Shin, J. H., and Lee, J. K. (2013) Up-down regulation of HO-1 and iNOS gene expressions by ethyl pyruvate via recruiting p300 to Nrf2 and depriving it from p65. *Free Radic. Biol. Med.* **65,** 468–476

34. Komatsu, M., Kurokawa, H., Waguri, S., Taguchi, K., Kobayashi, A., Ichimura, Y., Sou, Y. S., Ueno, I., Sakamoto, A., Tong, K. I., Kim, M., Nishito, Y., Iemura, S., Natsume, T., Ueno, T., Kominami, E., Motohashi, H., Tanaka, K., and Yamamoto, M. (2010) The selective autophagy substrate p62 activates the stress responsive transcription factor Nrf2 through inactivation of Keap1. *Nat. Cell Biol.* **12,** 213–223

35. Hall, E. T., and Bhalla, V. (2014) Is there a sweet spot for Nrf2 activation in the treatment of diabetic kidney disease? *Diabetes* **63,** 2904–2905

36. Zhang, D. D. (2013) Bardoxolone brings Nrf2-based therapies to light. *Antioxid. Redox Signal.* **19,** 517–518

37. To, C., Shilton, B. H., and Di Guglielmo, G. M. (2010) Synthetic triterpenoids target the Arp2/3 complex and inhibit branched actin polymerization. *J. Biol. Chem.* **285,** 27944–27957

38. Zoja, C., Benigni, A., and Remuzzi, G. (2014) The Nrf2 pathway in the progression of renal disease. *Nephrol. Dial. Transplant* **29,** i19–i24

39. Harris, R. C. (2013) The best-laid plans. *Am. J. Physiol. Renal Physiol.* **304,** F1086–F1087

40. Weerachayaphorn, J., Luo, Y., Mennone, A., Soroka, C. J., Harry, K., and Boyer, J. L. (2014) Deleterious effect of oltipraz on extrahepatic cholestasis in bile duct-ligated mice. *J. Hepatol.* **60,** 160–166